Oxidation of freestanding silicon nanocrystals probed with electron spin resonance of interfacial dangling bonds

R. N. Pereira,[1,*] D. J. Rowe,[2] R. J. Anthony,[2] and U. Kortshagen[2]

[1]*Department of Physics and Institute for Nanostructures, Nanomodelling and Nanofabrication, University of Aveiro, Campus Universitário de Santiago, P-3810-193 Aveiro, Portugal*

[2]*Department of Mechanical Engineering, University of Minnesota, Minneapolis, Minnesota 55455, USA*

(Received 24 November 2010; revised manuscript received 27 January 2011; published 28 April 2011)

The oxidation of freestanding silicon nanocrystals (Si-NCs) passivated with Si-H bonds has been investigated for a wide range of oxidation times (from a few minutes to several months) by means of electron spin resonance (ESR) of dangling bonds (DBs) naturally incorporated at the interface between the NC core and the developing oxide shell. These measurements are complemented with surface chemistry analysis from Fourier transform infrared spectroscopy. Two surface phenomena with initiation time thresholds of 15 min and 30 h are inferred from the dependence of ESR spectra on oxidation time. The first initiates before oxidation of surface Si−Si bonds and destruction of the NC hydrogen termination takes place (induction period) and results in a decrease of the DB density and a localization of the DB orbital at the central Si atom. Within the Cabrera-Mott oxidation mechanism, we associate this process with the formation of intermediate interfacial configurations, resulting from surface adsorption of water and oxygen molecules. The second surface phenomenon leads to a steep increase of the defect density and correlates with the formation of surface Si−O−Si bridges, lending experimental support to theoretically proposed mechanisms for interfacial defect formation involving the emission of Si interstitials at the interface between crystalline Si and the growing oxide.

DOI: 10.1103/PhysRevB.83.155327 PACS number(s): 61.46.Hk, 76.30.−v, 81.16.Pr

I. INTRODUCTION

Freestanding silicon nanocrystals (Si-NCs) are currently under intense investigation because they combine the unique features of Si at the nanoscale (for instance, wavelength-tunable light emission,[1] multiple exciton generation,[2] and possibility of doping[3–5]) with the versatile and inexpensive device fabrication associated with nanoparticle processing.[6] A variety of techniques have been used to produce freestanding Si-NCs, such as solid-gas reaction,[7] liquid-phase synthesis,[8,9] laser pyrolysis of silane,[10–13] laser ablation,[14] laser vaporization-controlled condensation,[15] and plasma-assisted decomposition of silane.[1,6,16,17] Among these, the latter silane plasma method has proved to be very efficient in producing large quantities of high-quality Si-NCs passivated with Si–H bonds (silane plasma Si-NCs) with control over diameter in the range 3–50 nm.[1,6,16]

Oxidation is one of the most important surface phenomena both from the fundamental and technological points of view. Oxidation of H-terminated Si-NCs can readily take place in air at room temperature,[5,18–22] whereas under pure molecular oxygen atmosphere higher temperatures are required.[23,24] Although efficient light emission from silane plasma Si-NCs in the range from near infrared to orange has been demonstrated,[1] the realization of green and blue light emission is necessary to materialize the full potential of Si-NCs. Theoretical work has shown that Si-NCs with diameters $d < 2.5$ nm should be capable of emitting green and blue light.[25–27] Unfortunately, the high-yield gas-phase methods of freestanding Si-NC fabrication based on plasma decomposition of silane are only efficient at producing NCs with diameters above 3 nm.[1,16] Surface oxidation is a promising means of reducing the crystalline core of these Si-NCs down to sizes where short-wavelength light emission is possible.[1] Hydrogen termination of the resulting surface-oxidized Si-NCs may be reestablished by wet etching of the oxide shell using hydrofluoric acid,[3,18] and further reduction of the Si-NCs size can be attained by repeating the oxidation-etching procedures. The formation of an oxide shell also transforms the as-grown Si-NCs (inherently hydrophobic due to the H termination) into hydrophilic NCs. In general, surface oxides are also responsible for the biocompatibility of materials used in medical applications.[28] Water solubility and biocompatibility are essential properties for Si-NCs since these are increasingly regarded as promising biomaterials.[29] In previous investigations of Si-NCs fabricated by other techniques, it has been found that oxidation may also result in a redshift of the NCs photoemission.[26,30,31] Theoretical calculations indicate that this could originate from the introduction of intragap energy levels by interfacial Si=O bonds[26,27,32] and Si–O–Si surface bridges.[33–35]

Although the crystalline core of silane plasma Si-NCs can be virtually defect free, coordination point defects are expected to form at the interface between the NC core and an oxide shell. Two types of interfacial paramagnetic defects have recently been detected with electron spin resonance (ESR) in gas-phase-grown NCs containing an oxide shell.[4] One was assigned to a structure similar to that of the so-called P_b centers in bulk-Si/SiO_2 interfaces, i.e., an sp^3 dangling bond (DB) on an interfacial Si atom, backbonded to three Si atoms of the Si crystal ($Si_3{\equiv}Si\bullet$).[36,37] The other defect was ascribed to a Si DB located in a disordered environment.[4] A total defect density of 5×10^{11} cm^{-2} was found,[4] which can be reduced ten times upon vacuum annealing.[38] Similar defects have been previously observed in porous silicon samples oxidized in ambient air.[39] Combined magnetic resonance and electrical studies demonstrated that these defects have an adverse impact as recombination and charge-trapping centers on the electrical conductivity of Si-NC ensembles[3,38] and on the efficiency of electronic doping with foreign atoms.[4] Importantly, degradation of light emission from confined excitons in silane plasma Si-NCs has been observed, which was attributed to an

oxidation-induced generation of DBs.[1,18] Earlier theoretical studies indicated that these defects are efficient photoluminescence quenchers.[25] On the other hand, luminescence enhancement has been observed after oxidation of Si-NCs produced by other methods, which has been attributed to an oxidation-induced passivation of DBs.[11,14,15,30,40–44] Distinct initial surface passivation and oxidation conditions may explain the apparent discrepancy between different studies. In an investigation where the oxidation approach of reducing the NCs size has been explored, the light emission of the smaller NCs obtained has been associated with defects,[1] in line with findings for Si nanocrystals embedded in amorphous SiO_2 (Ref. 45) and porous silicon.[46] Thus, a consensus has been reached that interfacial defects and, in particular, Si DBs influence strongly the (opto)electronic properties of Si-NC ensembles. If we are aware of the detailed dynamics and mechanisms of the creation and elimination of these defects during oxidation of silane plasma Si-NCs, we will be in a position to minimize their negative impact. Moreover, given the fact that these defects reside essentially at the interface between the crystalline Si core and the growing oxide shell, they are extremely sensitive interface probes and therefore provide invaluable insight into interface phenomena involved in oxidation of Si surfaces. However, despite their recognized worth, such studies have not been reported. In principle, one could rely on information obtained for H-terminated bulk-Si surfaces to infer the behavior of interfacial defects on silane plasma Si-NCs (H terminated). Because of its importance for the fabrication of electronic devices, the oxidation of bulk-Si has been widely investigated via a variety of experimental and theoretical methods.[47–55] However, studies monitoring the evolution DB interfacial defects upon oxidation of H-terminated bulk-Si surfaces have not been reported since the time scale of surface reactions in the early oxidation stages is shorter than the time required to acquire enough ESR scans to detect interfacial DB centers due to the relatively low density of these defects. As far as theoretical modeling is concerned, existing studies indicate that the P_b centers in bulk-Si/SiO_2 interfaces are a product of the emission of interfacial Si atoms to release strain generated due to the formation of Si−O−Si bonds.[47,48] To date, experimental evidence directly linking the creation of P_b defects with the formation of Si−O−Si bridges has been elusive.

In the present work, we use ESR recorded *in situ*, in combination with Fourier transform infrared (FTIR) spectroscopy, to study the oxidation of silane plasma Si-NCs. The present success in observing the dynamics of DB defects from a very early oxidation stage resulted from appropriate sample preparation and from the huge total surface provided by an ensemble of Si-NCs, as opposed to that of a bulk-Si sample. In this way, we gain knowledge of how oxidation influences the density and wave function of interfacial defects and correlate these with simultaneous changes at the surface structure.

II. EXPERIMENTAL DETAILS

Freestanding Si-NCs were synthesized in a nonthermal rf plasma with a frequency of 13.56 MHz and a power of 175 W. The flow rates of precursors were 6 standard cubic centimeters per minute (sccm) of silane and 200 sccm of argon. The reactor is a pyrex tube with a 22-mm internal diameter, and reactor pressure was held constant during synthesis at 3.6 Torr.[16] The crystalline diffraction pattern was measured using a Bruker-AXS microdiffractometer with a 2.2-kW sealed Cu x-ray source. An x-ray diffraction (XRD) pattern of as-grown Si-NCs is shown in curve (i) of Fig. 1, from which the mean NC diameter was calculated to be $d = 5.5 \pm 0.1$ nm using the Scherrer equation. For preparing samples for ESR measurements, the Si-NCs were collected from the plasma as a powder using a mesh, and for the FTIR measurements the Si-NCs were deposited from the plasma via inertial impaction onto gold-coated silicon substrates. To avoid oxidation, as-grown Si-NCs were transferred under vacuum condition from the synthesis reactor to a nitrogen-purged glovebox (oxygen and moisture level below 30 ppm), where further sample preparation for ESR and FTIR was carried out. For ESR measurements, a few milligrams of Si-NC powder was pressed into the bottom of ESR sample tubes (suprasil quartz, ~20 mm long), and afterward the open end of the tubes was sealed with epoxy glue in order to enable their transport from the glovebox to the ESR spectrometer without exposing the NCs to air. The transfer of the FTIR samples from the glovebox to the FTIR spectrometer was carried out using a gas-tight chamber that was sealed inside the glovebox. To initiate oxidation of the Si-NCs in the ESR and FTIR samples, we cleaved the top end of the ESR tubes in ambient air and opened the sample transport chamber to ambient air, respectively. The samples were immediately after introduced in the respective spectrometry apparatuses, and measurements were started. Our procedures allowed reducing the exposure time of the NCs to air down to 2 min before the first ESR or FTIR measurement was carried out. We estimate that the ambient pressures of water and oxygen are stabilized in Si-NC porous networks of the ESR and FTIR samples in only a few seconds after air exposure, and therefore, the diffusion of these molecules into the samples should not play a role in the discussion presented in this work. ESR measurements were performed at room temperature in continuous-wave Bruker spectrometers mounted with X-band microwave bridges. The spin-density measurements were calibrated using a diphenylpicrylhydrazyl (DPPH) reference, magnetic field values were measured using a nuclear magnetic resonance Teslameter

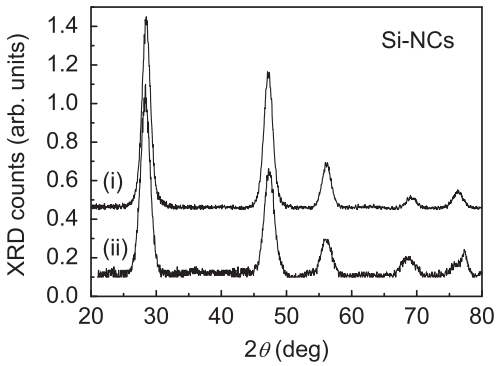

FIG. 1. XRD patterns recorded (i) for as-grown Si-NCs ($d = 5.5 \pm 0.1$ nm) and (ii) for the same NCs after *complete* oxidation ($d = 4.9 \pm 0.1$ nm).

(resolution better than 5×10^{-3} mT), and the microwave frequency was measured with a frequency counter with resolution above 0.00001 GHz. Under these experimental conditions, spin-density and g-value variations of at least 10% and 3×10^{-5}, respectively, can be distinguished. FTIR measurements were carried out with a nitrogen-purged Nicolet Series II Magna-IR System 750 spectrometer, equipped with a glowbar light source, a KBr beam splitter, and a mercury-cadmium-telluride detector. All absorbance spectra were recorded in diffuse reflection mode at room temperature with a resolution of 2 cm^{-1} and averaged over 100 scans. A bare gold-coated silicon wafer was used as a reference. The samples were exposed to air all the time between consecutive measurements.

III. EXPERIMENTAL DATA

A. Electron paramagnetic resonance

Figure 2 shows ESR spectra measured for a Si-NC sample at three different times of exposure to air (t_{ox}). The spectra show a structured band in the region of $g \simeq 2$, which can be well reproduced by a sum of an axially symmetric powder pattern of Lorentzian lines (dashed curves), whose linewidths increase linearly from the direction parallel to the symmetry axis to the perpendicular direction, and a relatively less intense line with Gaussian shape (dotted curves). The two spectral components originate from axially symmetric and isotropic defects with electron spin $S = 1/2$. The spectra obtained for the full range of oxidation times investigated, spanning from a few minutes to several months, were fitted with the two-component spectrum, from which the defect densities and ESR spectral parameters were extracted.[56] The obtained dependence of the defect density as a function of t_{ox} is depicted in Fig. 3(a). The contribution of axial defects is dominant since they always represent more than 85% of the total number of defects. The evolution of the parameters $g_\perp$ and $g_\parallel$ of the axial spectral component as a function of t_{ox} and their respective ESR peak-to-peak linewidths $\Delta B_{pp}^{\perp}$ and $\Delta B_{pp}^{\parallel}$ are shown in Fig. 4. As can be seen in Fig. 3(a), the defect density displays a decrease from 4.3×10^{10} to 3.1×10^{10} cm^{-2} over the first 10 h of air exposure. An increase of the defect density is observed for oxidation times above $t_{ox} \sim 30$ h, indicated by the dotted vertical lines in Figs. 3 and 4, followed by a saturation at about 5.5×10^{10} cm^{-2} at $t_{ox} \sim 800$ h (33 days), represented by the dashed vertical lines. As can be seen from Fig. 4, the values of $g_\perp = 2.0086$ and $g_\parallel = 2.0019$ observed after *complete* oxidation of the NCs ($t_{ox} > 800$ h) are very close to those reported for the $Si_3{\equiv}Si\bullet$ defects in bulk-Si/SiO_2 interfaces (P_b centers).[57,58] Thus, we assign the axial component of our spectra to a $Si_3{\equiv}Si\bullet$ defect in the interface between the NCs core and the growing oxide shell, denoted hereafter P_b^{NC} to distinguish from the P_b centers in bulk-Si/SiO_2 interfaces. The g value and peak-to-peak linewidth observed after *complete* oxidation for the isotropic spectral component are $g_D = 2.0053$ and $\Delta B_{pp}^{D} = 0.65$ mT, respectively, corresponding to spectrum (iii) in Fig. 2. These values are very close to those typically found for the Si DBs in a disordered environment, which have been observed in bulk-Si/SiO_2 interfaces,[59] and in amorphous Si.[60] Therefore,

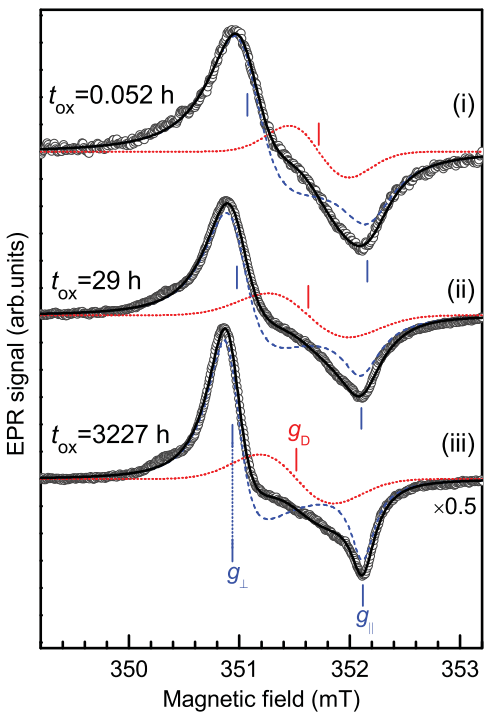

FIG. 2. (Color online) ESR spectra recorded with Si-NCs for different oxidation times t_{ox} (open circles), together with corresponding computer simulations (solid curves), taking into account a powder pattern of axial symmetry (dashed curves) and an isotropic resonance (dotted curves).

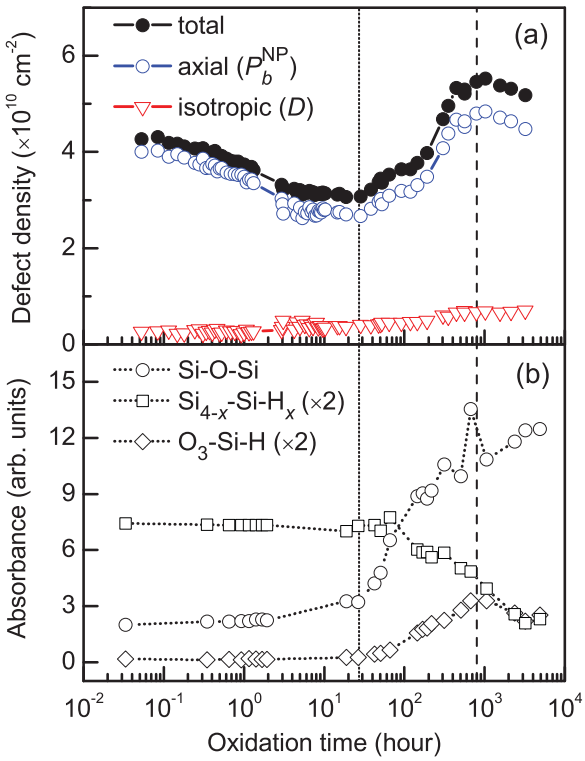

FIG. 3. (Color online) Dependence of (a) DB density and (b) intensity of FTIR bands from the surface species Si−O−Si, Si_{4-x}−Si−H_x, and O_3−Si−H as a function of t_{ox}.

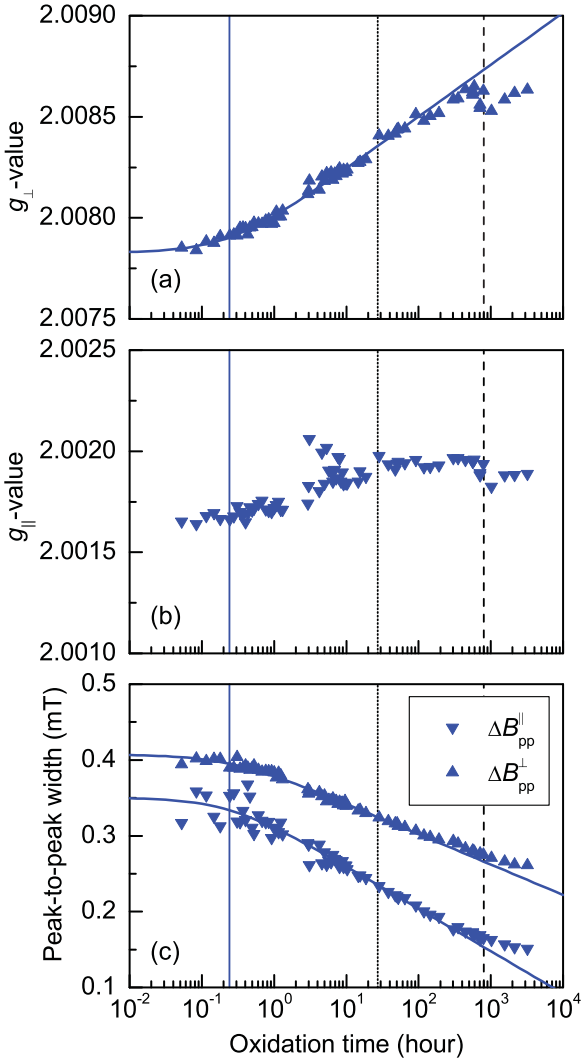

FIG. 4. (Color online) Evolution of ESR parameters (a) $g_\perp$, (b) $g_\parallel$, and (c) $\Delta B^{\perp}_{pp}$ and $\Delta B^{\parallel}_{pp}$ of the axial spectral component (P_b^{NC} centers) as a function of t_{ox}. Solid curves represent fits of the data for $t_{ox} < 200$ h with Elovich dependencies. The same value of characteristic time t_m, indicated by the vertical solid line, was considered for the three sets of data.

we assign this spectral component to the same type of defect in our Si-NCs.

B. Fourier transform infrared spectroscopy

Figure 5 shows sections of the FTIR spectra of Si-NCs recorded for different t_{ox}. In the first collected spectrum (within 0.033 h of air exposure), the spectral region of Si−H stretching modes is dominated by a structured band at 2000–2150 cm^{-1} due to Si_{4-x}−Si−H_x ($x = 1, 2, 3$) surface hydride groups.[1,3,6,18,19,61] In the lower energy range a band centered at 1045 cm^{-1} is observed, originating from Si−O−Si bridges.[1,3,18,19,61] The appearance of a small Si−O−Si band, as well as the observation of P_b-type defects, in the as-grown Si-NCs is most likely due to a small oxygen contamination of NCs during synthesis. A significant decrease of the hydride band is observed in the spectrum recorded for $t_{ox} = 218$ h, while the intensity of the band in the 1000–1250 cm^{-1} spectral

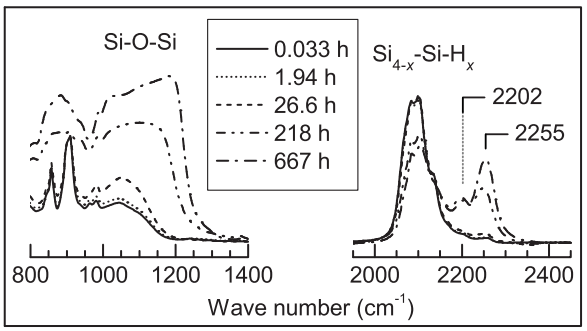

FIG. 5. Sections of FTIR spectra in the range of stretching modes of surface Si−O−Si and Si−H bonds recoded with Si-NCs for different oxidation times.

region due to Si−O−Si bonds displays a strong increase. These changes are accompanied by the emergence of a line at 2202 cm^{-1} due to Si−H stretching in intermediate oxidation states O_2−Si−H_2 and O_2Si−Si−H and a line at 2255 cm^{-1} from O_3−Si−H surface bonds.[3,19,61–63] A more detailed discussion of the origin of FTIR bands analyzed in the present study is given in Refs. 3, 18 and 19. The dependence of the intensity of the bands of Si−O−Si bonds, surface hydrides Si_{4-x}−Si−H_x, and O_3−Si−H surface bonds as a function of t_{ox} is shown in Fig. 3(b). The intensities of these bands were estimated by numerical integration of the spectra in the 995–1350, 1885–2145, and 2220–2400 cm^{-1} spectral intervals, respectively.

IV. DISCUSSION

An important point regarding the oxidation dynamics demonstrated by the data shown in Fig. 3(b) is that the surface of the Si-NCs is relatively stable against oxidation for many hours of air exposure. After a period of nearly 30 h characterized by a very slow oxidation, the oxidation accelerates in a logarithmic fashion until it reaches saturation at a long-term exposure of approximately 800 h. A crystalline core diameter $d = 4.9 \pm 0.1$ nm is estimated from the XRD pattern (Fig. 1) recorded after oxidation has reached saturation, indicating a growth of the oxide shell of about 0.3 ± 0.1 nm, in line with early observations for bulk-Si surfaces.[50,52] A slow-fast-slow evolution of Si−O−Si formation with $\log(t_{ox})$ has also been reported for ambient-air oxidation of bulk-Si surfaces terminated with hydrogen, with the initial period of slow oxidation, referred to as the *induction period*, ranging from 3 to 170 h (7 days), depending on the Si surface index, air humidity, and the initial amount of residual Si−OH groups at the surface.[49–52,54] It has been shown for bulk-Si surfaces that the duration of the induction period is shorter for higher air humidity and higher density of residual Si−OH groups.[52,54]

In the following, we assume that oxidation of our Si-NCs follows the Cabrera-Mott mechanism, as supported by previous investigations on similar Si-NCs.[5,19] This is the mechanism considered earlier in the description of the ambient-air oxidation of bulk-Si surfaces, i.e., in the simultaneous presence of water and oxygen molecules,[55] and is schematically represented in Fig. 6. Accordingly, the polar water molecules adsorb preferentially at surface silanol groups

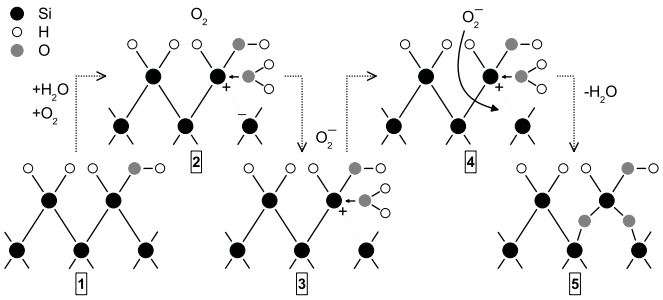

FIG. 6. Scheme of the steps that take place within the Cabrera-Mott theory in the early stages of ambient-air oxidation of a passivated Si surface (in the presence of water and oxygen molecules).

(step 2), to the detriment of the hydrophobic Si−H surface bonds.[52,54] These water molecules then aid in the cleavage of Si−Si backbonds of Si−OH due to their strong polarity (step 2). After this, an electron is transferred from the broken bond to an adsorbed O_2 molecule (step 3), and the resulting electrostatic potential forces the O_2^- to drift toward the cleaved Si−Si bond (step 4), leading to the oxidation of this bond and of a neighboring Si−Si bond (step 5).[55] The latter step initially involves the formation of a disilperoxo bridge Si−O−O−Si, which is subsequently transformed in the two Si−O−Si groups via Bartlett's butterfly mechanism.[55] Within the mechanism represented in Fig. 6, it is understood that the physical processes taking place prior to formation of Si−O−Si bridges (steps 1–4) are behind the existence of the induction period. We should also note that this model is fully compatible with the observed stability of the H termination of our NCs during the induction period.

As can be seen from Fig. 4, the shifts observed for the ESR parameters associated with the P_b^{NC} centers already occur during the induction period (i.e., for t_{ox} before the dotted lines in Fig. 4). Thus, changes of the defect environment during the early stages of air exposure are not due to formation of surface Si−O−Si bonds. These should rather be due to changes at the NC surface resulting from a configuration that is formed after adsorption of water and oxygen molecules takes place (steps 2–4 in Fig. 6). The dynamics of physical processes and reactions on solid surfaces can be described by the Elovich equation:[64]

$$n_m(t) = \lambda_m t_m \ln\left(1 + \frac{t}{t_m}\right), \tag{1}$$

where t is time, n_m is the amount of reaction products, and λ_m and t_m are reaction rate and characteristic time, respectively. Assuming a linear dependence between n_m and the ESR parameters $g_\perp$, $\Delta B_{pp}^\perp$, and $\Delta B_{pp}^\parallel$, the variation of these parameters with t_{ox} becomes proportional to $t_m \ln(1 + t_{ox}/t_m)$. The results of fitting the dependence of $g_\perp$, $\Delta B_{pp}^\perp$, and $\Delta B_{pp}^\parallel$ on t_{ox} with such a dependence are shown in Fig. 4 as solid lines. As can be seen, for t_{ox} below 800 h (33 days), i.e., before the P_b^{NC} density and Si−O−Si bond formation reach saturation, the three sets of data are well described by Elovich dependencies with the same value of characteristic time $t_m = 0.24$ h (14.4 min). This shows that the observed changes in ESR parameters most likely result from the same surface process.

The ESR parameters are closely related to the electronic and microscopic structures of paramagnetic states. From the deviation of the g values from the free-electron value g_e, due to spin-orbit coupling, changes on the electronic structure of the P_b^{NC} defects can be inferred. The values of the g tensor can be approximated using the expression[65]

$$g_{\alpha\beta} = g_e + 2\sum_{n\neq 0} \frac{\sum_k \langle 0|L_\alpha^k|n\rangle \lambda_k \langle n|L_\beta^k|0\rangle}{\varepsilon_0 - \varepsilon_n}, \tag{2}$$

where $|0\rangle$ and $|n\rangle$ are the DB wave functions of the ground and the excited states, respectively, ε_0 and ε_n are the energies of the ground and excited states, respectively, λ_k is the spin-orbit coupling constant of atom k neighboring the DB, which depends on its position relative to that atom, and $L_{\alpha,\beta}^k$ are components ($\alpha,\beta = x,y,z$) of the orbital angular momentum operator with respect to the position of atom k. Here we consider the axis of symmetry to be the z axis, i.e., $g_\parallel \equiv g_{zz}$ and $g_\perp \equiv g_{xx} = g_{yy}$. The ground-state wave function of the unpaired electron $|0\rangle$ can be constructed as a linear combination of $3s$ and $3p$ atomic orbitals of Si, denoted $|s\rangle$ and $|p\rangle$, respectively, centered on the atom sites near the DB:[66]

$$|0\rangle = \sum_k \eta_k(\sigma_k|s\rangle + \pi_k|p\rangle), \tag{3}$$

where the coefficients η_k, σ_k, and π_k obey the normalization conditions $\sum_k \eta_k^2 = 1$ and $\sigma_k^2 + \pi_k^2 = 1$ for all k.[67] It is obvious that s orbitals do not contribute to the shift of g from g_e because $L_{\alpha,\beta}^k|s\rangle = 0$. From previous investigations,[36,66–68] we know that the $3s$-$3p$ hybridization at the central Si atom ($k = 1$) for centers with the same $Si_3{\equiv}Si\bullet$ structure is quite insensitive to the specific environment of the defect since very distinct centers, such as the E center in Si,[66] the P_b centers in bulk-Si/SiO_2,[36,67] and the D centers,[68] are characterized by very similar $3s$ and $3p$ hybridization components of $\sigma_1^2 = 0.06$–0.14 and $\pi_1^2 = 0.86$–0.94, respectively. Thus, changes on the unpaired-electron hybridization ratio should not account for the observed behavior of $g_\parallel$ and $g_\perp$ upon air exposure. Hereafter, we assume constant values of $\sigma_1^2 = 0.1$ and $\pi_1^2 = 0.90$ for these parameters. The value η_1^2 represents the probability density of the unpaired electron at the central site of the DB. For P_b defects in various types of thermal (111) and (100)Si/SiO_2 interfaces and in oxidized porous Si, this is found to be in the range $\eta_1^2 = 0.58$–0.67,[36] with the remaining probability density distributed among the neighboring sites. Hence, the wave function of P_b centers consists almost of a $3p_z$ orbital $|p_z\rangle$ located on the central Si atom. This leads to the fact that, for this type of center, $(g_\parallel - g_e) \sim 0$ since the terms $\langle n|L_z^k|0\rangle$ in Eq. (2) are very small because $\langle p_\alpha|L_z|p_\beta\rangle$ is nonzero only when $\alpha = \beta$ and the contribution of $|p_z\rangle$ to $|n\rangle$ is small. In contrast, $(g_\perp - g_e)$ has a larger value because $\langle n|L_{x,y}^k|p_z\rangle \neq 0$. This is also valid in the full range of g values observed for our P_b^{NC} centers, where $|\, g_\perp - g_e\,| = 0.0055$–$0.0063$ is about one order of magnitude above $|\, g_\parallel - g_e\,| = 0.0005$–$0.0007$. In a previous study,[66] Watkins and Corbett have carried out a simplified calculation of $g_\parallel$ and $g_\perp$ for $Si_3{\equiv}Si\bullet$ centers considering only the Si central atom and its three nearest neighbors and only the dominant first-order term in the spin-orbit interaction, i.e., only $k = 1$ in Eq. (2). In their model, simple one-electron bonding

and antibonding molecular orbitals between the central atom and its neighbors were used as approximations to the excited localized valence and conduction band states in the sum of Eq. (2). The calculation led to the results[66]

$$g_{\parallel} = g_e, \tag{4}$$

$$g_{\perp} = g_e + \lambda_1 \gamma_1^2 \left(\frac{1}{E_b} - \frac{1}{E_a} \right), \tag{5}$$

where E_a and E_b are the energies of the bonding and antibonding orbitals, respectively, and γ_1^2 is the probability density of the $3p_z$ orbital at the central Si site, which, according to Eq. (3), can be approximated to $\gamma_1^2 \approx \eta_1^2 \pi_1^2$. As readily expected, the model predicts a zero deviation of $g_{\parallel}$ from g_e, which explains the relatively weak change of $g_{\parallel}$ upon oxidation of the NCs compared to $g_{\perp}$. From the initial value of $g_{\perp} = 2.0078$, corresponding to spectrum (i) in Fig. 2, to the saturation value of $g_{\perp} = 2.0086$, the $g_{\perp}$ value displays a total change of $\Delta g_{\perp} = 0.0008$. In contrast, a much smaller change of $\Delta g_{\parallel} = 0.0002$ is observed for $g_{\parallel}$ over the same period of t_{ox}. Assuming a negligible variation of $(1/E_b - 1/E_a)$ and taking into account a constant π_1^2 as discussed above, the increase of $g_{\perp}$ with t_{ox} can be understood in terms of an enhancement of the localization of the unpaired-electron density on the central Si atom, i.e., an increase in η_1^2. The increase of $g_{\perp}$ with the localization of the unpaired electron can also be qualitatively understood from Eq. (2) since a larger density of the $3p_z$ orbital at the DB site will result in larger contribution of $L_{x,y}|p_z\rangle$. Using Eq. (5) and the data shown in Fig. 4(a), we estimate that the unpaired-electron wave function becomes ~15% more localized on the central Si atom after *complete* oxidation of the NC surface. This value could correspond to a lower limit of the unpaired-electron localization since such localization could lead to a small decrease of the term $(1/E_b - 1/E_a)$. Since $g_{\perp}$ is larger than g_e, the term $(1/E_b - 1/E_a)$ is positive and $E_b < E_a$. A localization of the defect state is expected to lead to a deepening of its energy level,[69,70] i.e., an increase of E_b and a decrease of E_a, which would lower the $(1/E_b - 1/E_a)$ term in Eq. (5). Larger $g_{\perp}$ have also been associated with an enhanced localization of the unpaired-electron state in previous studies to explain the larger $g_{\perp}$ of P_b centers in bulk-Si/SiO_2 compared to the g value of D centers[68] and to explain the increase of $g_{\perp}$ of surface Si DBs observed upon low-pressure oxidation of an unpassivated bulk-Si surface.[71]

We shall now discuss the changes in the widths $\Delta B_{pp}^{\parallel}$ and $\Delta B_{pp}^{\perp}$ with t_{ox}, shown in Fig. 4(b). Previous studies carried out in different bulk-Si/SiO_2 interfaces have concluded that the ESR linewidths of P_b centers consist mainly of three superimposed contributions: (i) a component due to strain-induced distributions of $g_{\parallel}$ and $g_{\perp}$, (ii) a component due to unresolved ^{29}Si superhyperfine interactions, and (iii) a component due to dipolar broadening, resulting from dipole-dipole interactions among the unpaired electrons.[37,72] As discussed above, the widths $\Delta B_{pp}^{\parallel}$ and $\Delta B_{pp}^{\perp}$ display similar dependencies with t_{ox} (see Fig. 4), and thus, the origin of the changes is most probably the same. If these changes would result from variations in the strain-induced component (i), these should be much stronger for $\Delta B_{pp}^{\perp}$ than for $\Delta B_{pp}^{\parallel}$ because $g_{\perp}$ is much more sensitive to strain than $g_{\parallel}$, as readily discussed in Ref. 37. We observe similar changes of 0.19 ± 0.03 mT and 0.14 ± 0.01 mT for $\Delta B_{pp}^{\parallel}$ and $\Delta B_{pp}^{\perp}$, respectively, over the entire time span of the experiments, and therefore, we can discard effect (i) as the one responsible for the linewidth variation. We can also rule out that these variations originate from changes in the dipolar broadening component (iii) because in such a case an increase in defect density should be accompanied by an increase of ΔB_{pp} and vice versa, which is in clear contrast with our experimental data. The decrease of $\Delta B_{pp}^{\parallel}$ and $\Delta B_{pp}^{\perp}$ with t_{ox} could result in part from changes of the line broadening component (ii), originating from unresolved superhyperfine interactions of the unpaired-electron spin with the nuclear spin of atoms neighboring the central Si site. In the case of P_b centers, values in the range 0.5–0.1 mT are expected for the superhyperfine splitting with five different Si sites in the vicinity of the central Si atom.[73] According to the localization effect discussed above, the enhancement of the localization of the unpaired-electron density on the central Si atom is accompanied by a decrease of electron-density probability at the neighboring atomic sites, i.e., a decrease of η_k for $k > 1$ as a result of the normalization condition $\sum_k \eta_k^2 = 1$. The splitting of the spin energy states due to the superhyperfine interaction is proportional to the DB wave-function coefficient η_k at the corresponding atom. The decrease in the coefficients η_k (for $k > 1$) leads to a narrowing of the superhyperfine splitting with each individual atomic site and, consequently, to a reduction of the spread of the ESR resonances which contain such unresolved structure. Although a Gaussian line shape is usually expected for unresolved superhyperfine interaction, a group of researchers found that for P_b defects in bulk-Si/SiO_2 the linewidth component assigned to unresolved superhyperfine structure is better described by a Voigt line shape (convolution of Lorentzian and Gaussian line broadening).[74] Moreover, in a later detailed investigation of P_b ESR linewidths, the same group successfully approximated the superhyperfine broadening component to a purely Lorentzian line shape.[37] On the other hand, we cannot rule out an additional contribution to the linewidth resulting from spin-lattice relaxation, which seems to be absent in ESR lines of previous P_b defect studies in bulk-Si/SiO_2 (Refs. 74 and 37) since the spin relaxation mechanisms in our P_b^{NC} centers (before *complete* formation a surface oxide) may be different. Moreover, our *in situ* oxidation measurements have been carried out at room temperature, in contrast to the previous studies of P_b centers performed at liquid-helium temperatures.[37,74] A spin-lattice relaxation component would contribute to the line shape has a Lorentzian broadening. A decrease in such a broadening component could also contribute to the observed decrease of the linewidth with t_{ox}. A decrease of the width of ESR lines from surface Si DBs has also been reported to occur upon oxidation of unpassivated bulk-Si surfaces.[71] In Ref. 71, this linewidth narrowing has been associated with an increase of the spin-lattice relaxation time, which resulted from an oxidation-induced localization of the unpaired-electron state.[71] A similar effect could take place in our case, where the localization of the DB state discussed above would lead to a longer spin-lattice relaxation time. We would like to note that should adsorbed oxygen molecules have an effect on the ESR linewidths, these would be expected to result in a line broadening[75] and therefore cannot account for our observations. Oxygen molecules (paramagnetic) in

the vicinity of paramagnetic states provide an efficient spin relaxation path, which results in a shortening of spin relaxation times and, consequently, in a linewidth increase.[75]

As mentioned above, we assign the changes in the P_b^{NC} defect environment, which lead to the defect localization, to changes at the NC surface resulting from a configuration that is formed after adsorption of water and oxygen molecules and before surface Si−O−Si bonds are formed (steps 2–4 in Fig. 6). However, it is difficult to establish which of the possible configurations associated with the steps 2–4 is responsible for these changes. Nonetheless, it is reasonable to assume that surface configurations associated with steps 2 and 3 lead to a localization of P_b^{NC} DB charges since those configurations will result in a polarization of the interface region, pushing electron density toward the Si atom where the DB is located. The decrease of DB density observed in the early stages of air exposure should also result from a surface reaction that takes place before formation of Si−O−Si bridges. In a previous study of photoluminescence (PL) from confined exciton recombination in Si-NCs present in freshly prepared porous silicon, a two-stage behavior of the PL intensity as a function of oxidation time has been observed.[30] Namely, an initial PL increase, which has been interpreted as resulting from passivation of DB defects, was followed by a PL quenching due to oxygen-related surface states formed during oxidation.[30] Our experimental data seem to support this interpretation. However, the two studies cannot be directly compared due to the vastly different Si-NC preparation methods and oxidation conditions applied. The surface process behind the observed initial decrease of the DB density in our Si-NCs is not clear. This could result from an effective passivation of DBs via, e.g., the reaction $Si_3{\equiv}Si\bullet + H_2O \rightarrow Si_3{\equiv}Si{-}OH + H$. On the other hand, it could also result from a charge transfer process involving the surface configurations associated with step 3 in Fig. 6, where the unpaired electron of the DB (not represented) is captured at the positively charged site of the broken bond. Here the Si−Si bond is restored, and the DB defect becomes positively charged and, therefore, undetectable by ESR. Clarification of whether these processes are energetically favorable may be provided by future studies based on first-principles calculations.

From comparison of the data shown in Figs. 3(a) and 3(b), it is clear that the increase of the density of interfacial P_b^{NC} defects is accompanied by a simultaneous increase of the Si−O−Si vibrational band intensity, supporting previous theoretical studies of P_b defect formation.[47,48] First-principles studies of bulk-Si surfaces have predicted that strong local stress arises around Si−O−Si bridges formed during oxidation.[53] To release the stress, Si atoms participating in newly formed Si−O−Si bonds are emitted, leaving behind a bridge-bond oxygen (BBO) and unsatisfied orbitals at nearest-neighboring silicon atoms.[53] These dangling orbitals may form bonds between them[53] or remain unsaturated as P_b centers,[47,48] depending on the location of BBO formation. Our data provide compelling experimental evidence in support of the surface phenomena that theory predicts to take place during oxidation of the H-passivated Si surface.[47,48] We should mention that the oxidation-induced increase of DB density takes place in our Si-NCs (H passivated), but the opposite may occur in unpassivated (or only partially passivated) Si-NCs containing an initially high density of defects. In this situation, oxidation could result in a reduction of defects, as previously observed in the case of unpassivated bulk-Si surfaces.[71]

V. CONCLUSIONS

The oxidation of H-passivated silane plasma Si-NCs was probed by means of *in situ* ESR of interfacial DBs and surface structure analysis from FTIR spectroscopy. Our data allow important conclusions regarding fundamental aspects of Si-NC oxidation. Two surface processes with initiation time thresholds of about 15 min and 30 h were identified. The first process leads to a decrease of the defect density and to a localization of the interfacial DB wave function at the central Si site, consistent with the observed increase of $g_\perp$ and decrease of ESR linewidths associated with the paramagnetic state. From analysis of the experimental data within the Cabrera-Mott oxidation theory, we assign this process to the formation of intermediate surface configurations resulting from adsorption of water and oxygen molecules, which takes place before surface Si−O−Si bonds are formed. The second process leads to an increase of the interfacial defect density and correlates with the formation of surface Si−O−Si bridges, lending experimental support to theoretically proposed mechanisms of P_b defect formation,[47,48] involving the emission of Si interstitials at stressed Si−O−Si interfacial bonds.

ACKNOWLEDGMENTS

D.J.R. and R.J.A. were primarily supported by the MRSEC program of the National Science Foundation (NSF) under Award No. DMR-0819885. This program is also acknowledge for supporting a working visit of R.N.P. to the University of Minnesota. Part of this work was carried out in the College of Science and Engineering Characterization Facility, University of Minnesota, which has received capital equipment funding from the NSF through the MRSEC, ERC, and MRI programs, in the College of Science and Engineering and Nanofabrication Center, University of Minnesota, which receives partial support from NSF through the NNIN program, and at the Institute for Nanostructures, Nanomodelling and Nanofabrication in Portugal with funding from the HybridSolar Project. The authors would also like to acknowledge the Biophysical Spectroscopy Facility, University of Minnesota, David D. Thomas, and Ryan Mello for their support with ESR apparatus and José Coutinho for fruitful discussions.

*rnpereira@ua.pt

[1] A. Gupta, M. T. Swihart, and H. Wiggers, Adv. Funct. Mater. **19**, 696 (2009).

[2] M. C. Beard, K. P. Knutsen, P. Yu, J. M. Luther, Q. Song, W. K. Metzger, R. J. Ellingson, and A. J. Nozik, Nano Lett. **7**, 2506 (2007).

[3] A. R. Stegner, R. N. Pereira, K. Klein, R. Lechner, R. Dietmueller, M. S. Brandt, M. Stutzmann, and H. Wiggers, Phys. Rev. Lett. **100**, 026803 (2008).
[4] A. R. Stegner, R. N. Pereira, R. Lechner, K. Klein, H. Wiggers, M. Stutzmann, and M. S. Brandt, Phys. Rev. B **80**, 165326 (2009).
[5] X. D. Pi, R. Gresback, R. W. Liptak, S. A. Campbell, and U. Kortshagen, Appl. Phys. Lett. **92**, 123102 (2008).
[6] L. Mangolini and U. Kortshagen, Adv. Mater. **19**, 2513 (2007).
[7] J. Acker, K. Bohmhammel, E. Henneberg, G. Irmer, I. Röver, and G. Roewer, Adv. Mater. **12**, 1605 (2000).
[8] J. R. Heath, Science **258**, 1131 (1992).
[9] R. A. Bley and S. M. Kauzlarich, J. Am. Chem. Soc. **118**, 12461 (1996).
[10] G. Ledoux, J. Gong, F. Huisken1, O. Guillois, and C. Reynaud, Appl. Phys. Lett. **80**, 4834 (2002).
[11] G. Ledoux, O. Guillois, D. Porterat, C. Reynaud, F. Huisken, B. Kohn, and V. Paillard, Phys. Rev. B **62**, 15942 (2000).
[12] X. Li, Y. He, S. S. Talukdar, and M. T. Swihart, Langmuir **19**, 8490 (2003).
[13] F. Hua, M. T. Swihart, and E. Ruckenstein, Langmuir **21**, 6054 (2005).
[14] V. Švrček, T. Sasaki, Y. Shimizu, and N. Koshizaki, Appl. Phys. Lett. **89**, 213113 (2006).
[15] S. Li, S. J. Silers, and M. S. El-Shall, J. Phys. Chem. B **101**, 1794 (1997).
[16] L. Mangolini, E. Thimsen, and U. Kortshagen, Nano Lett. **5**, 655 (2005).
[17] Y. Kanemitsu, S. Okamoto, M. Otobe, and S. Oda, Phys. Rev. B **55**, R7375 (1997).
[18] X. D. Pi, L. Mangolini, S. A. Campbell, and U. Kortshagen, Phys. Rev. B **75**, 085423 (2007).
[19] R. W. Liptak, U. Kortshagen, and S. A. Campbell, J. Appl. Phys. **106**, 064313 (2009).
[20] I. Umezu, A. Sugimura, T. Makino, M. Inada, and K. Matsumoto, J. Appl. Phys. **103**, 024305 (2008).
[21] D.-Q. Yang, J.-N. Gillet, M. Meunier, and E. Sacher, J. Appl. Phys. **97**, 024303 (2005).
[22] I. N. Germanenko, M. Dongol, Y. B. Pithawalla, M. S. El-Shall, and J. A. Carlisle, Pure Appl. Chem. **72**, 245 (2000).
[23] J. Holm and J. T. Roberts, Langmuir **23**, 11217 (2007).
[24] Y.-C. Liao, A. M. Nienow, and J. T. Roberts, J. Phys. Chem. B **110**, 6190 (2006).
[25] C. Delerue, G. Allan, and M. Lannoo, Phys. Rev. B **48**, 11024 (1993).
[26] M. V. Wolkin, J. Jorne, P. M. Fauchet, G. Allan, and C. Delerue, Phys. Rev. Lett. **82**, 197 (1999).
[27] A. Puzder, A. J. Williamson, J. C. Grossman, and G. Galli, Phys. Rev. Lett. **88**, 097401 (2002).
[28] S. Piscanec, L. C. Ciacchi, E. Vesselli, G. Comelli, O. Sbaizero, and S. M. A. De Vita, Acta Mater. **52**, 1237 (2004).
[29] M. H. Nayfeh, E. V. Rogozhina, and L. Mitas, in *Synthesis, Functionalization and Surface Treatment of Silicon Nanoparticles*, edited by M. I. Barton (American Scientific, Stevenson Ranch, CA, 2003), p. 173.
[30] K. Dohnalová, K. Kůsová, and I. Pelant, Appl. Phys. Lett. **94**, 211903 (2009).
[31] J. S. Biteen, N. S. Lewis, H. A. Atwater, and A. Polman, Appl. Phys. Lett. **84**, 5389 (2004).
[32] M. Luppi and S. Ossicini, Phys. Rev. B **71**, 035340 (2005).
[33] I. Vasiliev, J. R. Chelikowsky, and R. M. Martin, Phys. Rev. B **65**, 121302(R) (2002).
[34] M. Nishida, Phys. Rev. B **69**, 165324 (2004).
[35] R. J. Eyre, J. P. Goss, and P. R. Briddon, Phys. Rev. B **76**, 245325 (2007).
[36] A. Stesmans, B. Nouwen, and V. V. Afanas'ev, Phys. Rev. B **58**, 15801 (1998).
[37] D. Pierreux and A. Stesmans, Phys. Rev. B **66**, 165320 (2002).
[38] S. Niesar, A. R. Stegner, R. N. Pereira, M. Hoeb, H. Wiggers, M. S. Brandt, and M. Stutzmann, Appl. Phys. Lett. **96**, 193112 (2010).
[39] M. Schoisswohl, J. L. Cantin, H. J. von Bardeleben, and G. Amato, Appl. Phys. Lett. **66**, 3660 (1995).
[40] B. Gelloz, A. Kojima, and N. Koshida, Appl. Phys. Lett. **87**, 031107 (2005).
[41] B. K. Meyer, V. Petrova-Koch, T. Muschik, H. Linke, P. Omling, and V. Lehmann, Appl. Phys. Lett. **63**, 1930 (1993).
[42] G. Ledoux, J. Gong, and F. Huisken, Appl. Phys. Lett. **79**, 4028 (2001).
[43] L. N. Dinh, L. L. Chase, M. Balooch, W. J. Siekhaus, and F. Wooten, Phys. Rev. B **54**, 5029 (1996).
[44] F. Huisken, B. Kohn, and V. Paillard, Appl. Phys. Lett. **74**, 3776 (1999).
[45] S. Godefroo, M. Hayne, M. Jivanescu, A. Stesmans, M. Zacharias, O. I. Lebedev, G. Van Tendeloo, and V. V. Moshchalkov, Nature Nanotechnology **3**, 174 (2008).
[46] S. M. Prokes and W. E. Carlos, J. Appl. Phys. **78**, 2671 (1995).
[47] T. Yamasaki, K. Kato, and T. Uda, Phys. Rev. Lett. **91**, 146102 (2003).
[48] K. Kato, T. Yamasaki, and T. Uda, Phys. Rev. B **73**, 073302 (2006).
[49] M. R. Houston and R. Maboudian, J. Appl. Phys. **78**, 3801 (1995).
[50] D. Gräf, M. Grundner, R. Schulz, and L. Mühlhoff, J. Appl. Phys. **68**, 5155 (1990).
[51] D. Bodlaki and E. Borguet, J. Appl. Phys. **95**, 4675 (2004).
[52] T. Miura, M. Niwano, D. Shoji, and N. Miyamoto, J. Appl. Phys. **79**, 4373 (1996).
[53] H. Kageshima and K. Shiraishi, Phys. Rev. Lett. **81**, 5936 (1998).
[54] M. Niwano, J. Kageyama, K. Kurita, K. Kinashi, I. Takahashi, and N. Miyamoto, J. Appl. Phys. **76**, 2157 (1994).
[55] G. F. Cerofolini, D. Mascolo, and M. O. Vlad, J. Appl. Phys. **100**, 054308 (2006), and references therein.
[56] A small unidentified shoulder at a magnetic field of ∼350.5 mT can be distinguished in the spectra recorder for longer oxidation times. We observe that the inclusion of this small resonance in the fitting procedure does not result in a sensible change in the ESR parameters obtained for the dominant components P_b^{NC} and D, as a result of the small intensity of this line, which is about 150 times less intense than the P_b^{NC} component, and the first derivative nature of ESR lines, where the effects of the positive and negative sides of the line on the fitting calculation compensate each other. Therefore, for the sake of simplicity and consistency, we did not included this small shoulder in our simulation of the spectra.
[57] A. Stesmans and V. V. Afanas'ev, J. Appl. Phys. **83**, 2449 (1998), and references therein.
[58] E. Poindexter, P. Caplan, B. Deal, and R. Razouk, J. Appl. Phys. **52**, 879 (1981).
[59] T. Wimbauer, K. Ito, Y. Mochizuki, M. Horikawa, T. Kitano, M. S. Brandt, and M. Stutzmann, Appl. Phys. Lett. **76**, 2280 (2000).
[60] M. H. Brodsky and R. S. Title, Phys. Rev. Lett. **23**, 581 (1969).

[61] W. Theiss, Surf. Sci. Rep. **29**, 91 (1997).
[62] Y. Kato, T. Ito, and A. Hiraki, Jpn. J. Appl. Phys. **27**, L1406 (1988).
[63] G. Lucovsky, J. Yang, S. S. Chao, J. E. Tyler, and W. Czubatyj, Phys. Rev. B **28**, 3225 (1983).
[64] C. Aharoni and F. C. Tompkins, Adv. Catal. **21**, 1 (1970).
[65] A. J. Stone, Proc. R. Soc. London, Ser. A **271**, 424 (1963).
[66] G. D. Watkins and J. W. Corbett, Phys. Rev. **134**, A1359 (1964).
[67] K. L. Brower, Appl. Phys. Lett. **43**, 1111 (1983).
[68] T. Umeda, S. Yamasaki, J. Isoya, and K. Tanaka, Phys. Rev. B **59**, 4849 (1999).
[69] A. M. Stoneham, *Theory of Defects in Solids* (Clarendon Press, Oxford, 1975).
[70] M. Lannoo and J. Bourgoin, *Point Defects in Semiconductors I: Theoretical Aspects* (Springer-Verlag, Berlin, 1981).
[71] T. Umeda, M. Nishizawa, T. Yasuda, J. Isoya, S. Yamasaki, and K. Tanaka, Phys. Rev. Lett. **86**, 1054 (2001).
[72] K. L. Brower, Phys. Rev. B **33**, 4471 (1986).
[73] G. Van Gorp and A. Stesmans, Phys. Rev. B **45**, 4344 (1992).
[74] A. Stesmans and G. Van Gorp, Phys. Rev. B **42**, 3765 (1990).
[75] C. P. Poole, *Electron Spin Resonance: A Comprehensive Treatise on Experimental Techniques* (Dover, Mineola, NY, 1983).